Dual Pulsed Laser Deposition system for the growth of complex materials and heterostructures

P. Orgiani [1,2] S. Kumar Chaluvadi [1,2] S. Punathum Chalil [1,2] F. Mazzola [1,3] A. Jana [1,2] S. Dolabella [1] P. Rajak [1,2] M. Ferrara,[1] D. Benedetti [1] A. Fondacaro,[1] F. Salvador,[1] R. Ciancio [4] J. Fujii [1] G. Panaccione [1] I. Vobornik [1] and G. Rossi [1,5]

[1)]CNR-IOM Istituto Officina dei Materiali, TASC Laboratory, Areas Science Park, s.s.14 km 163.5, I-34149 Trieste, Italy

[2)]International Centre for Theoretical Physics (ICTP), Str. Costiera 11, I-34151 Trieste, Italy

[3)]Department of Molecular Sciences and Nanosystems, Ca' Foscari University of Venice, 30172 Venice, Italy

[4)]AREA Science Park, Padriciano 99, I-34149 Trieste, Italy

[5)]Department of Physics, University of Milano, Via Celoria 16, I-20133 Milano, Italy

(*Electronic mail: pasquale.orgiani@cnr.it)

(Dated: 16 December 2024)

Here we present an integrated ultra-high-vacuum (UHV) apparatus for the growth of complex materials and heterostructures. The specific growth technique is the Pulsed Laser Deposition (PLD) by means of a dual-lasers source based on an excimer KrF ultra-violet and solid-state Nd:YAG infra-red lasers. By taking advantage of the two laser sources - both lasers can be independently used within the deposition chambers - a large number of different materials - ranging from oxides to metals, to selenides and others - can be successfully grown in the form of thin films and heterostructures. All of the samples can be in-situ transferred between the deposition chambers and the analysis chambers by using vessels and holders' manipulators. The apparatus also offers the possibility to transfer samples to remote instrumentation, under UHV conditions by means of commercially available UHV-suitcases. The Dual-PLD operates for in-house research as well as user facility in combination with the Advanced Photo-electric Effect (APE) beamline at the Elettra synchrotron radiation facility in Trieste and allows synchrotron-based photo-emission as well as x-ray absorption experiments on pristine films and heterostructures.

I. INTRODUCTION

Quantum materials exhibit unique physical phenomena, especially at the interface in heterostructures with other functional materials and/or at their surfaces[1–4]. Such a result is a direct consequence of the recent progress of thin film technology which is nowadays capable to provide multi-layered heterostructures with structural properties comparable to those observed in single-crystals[5–7]. In this respect, Pulsed Laser Deposition (PLD) growth technique has clearly been demonstrated to be extremely efficient as well as tremendously flexible in growing thin film and heterostructures of quantum materials[8–12]. The main characteristic of a PLD system is the capability to grow materials at a wide range of ambient pressure (up to 1 mbar). As a matter of fact, differently from other deposition techniques such as Molecular Beam Epitaxy (MBE) or Sputtering, the single-atomic species are supplied through an ablation process of a target in form of polycrystalline powders and/or single crystal by the irradiation of a high-intense laser beam. Since the laser pulse duration (about 20 ns) is much shorter than the heat diffusion time, the energy of the laser pulse is realized by the breaking of the molecular links among the different atoms on the material surface thus resulting in the *ablation* regardless of this last. The use of the PLD technique also allows the deposition of materials/elements characterized by an extremely high evaporation/sublimation temperature, which prevents their deposition by conventional MBE. For instance, this is the case of the strontium ruthenate $SrRuO_3$ compound, which is generally used as a metallic electrode as well as itinerant ferromagnetic material in perovskite heterostructures and is very efficiently deposited by PLD[13]. The ablation process does not require any carrier gas for the deposition process (e.g. noble gas or oxygen for the sputtering[14]) and the propagation of the ablated plume of materials is stopped only at very high pressure (i.e. several mbar) thus making the deposition process possible at those background pressure conditions (which are, for instance, limited up to 10^{-5} mbar for MBE system[5,15]). Over the last decades, we have therefore witnessed a tremendous effort by the material science community to develop the ability to grow, probe, control, and investigate the structural as well as the electronic properties of quantum materials, in particular when piled up in form of digital heterostructures[16].

We here report on an innovative system of the growth of thin film by PLD which takes advantage of two independent laser sources - namely an excimer KrF ultra-violet (UV) and a solid-state Nd:YAG infra-red (IR) one[17]. Our system - named Dual-PLD - has been able to deposit tens of different materials in form of thin films and/or heterostructures with very high structural quality. Those materials have not been limited to oxides[18–20] – for which the merits of PLD are well-acknowledged – but also selenides, dichalcogenides and pure metals[21–23]. Moreover, being directly connected to the Advanced Photo-electric Effect (APE) experiments beamline[24] at Elettra synchrotron radiation facility within the same ultra-high-vacuum (UHV) manifold, all of the surface-contamination problems have been avoided and surface-sensitive experiments have been allowed on untreated
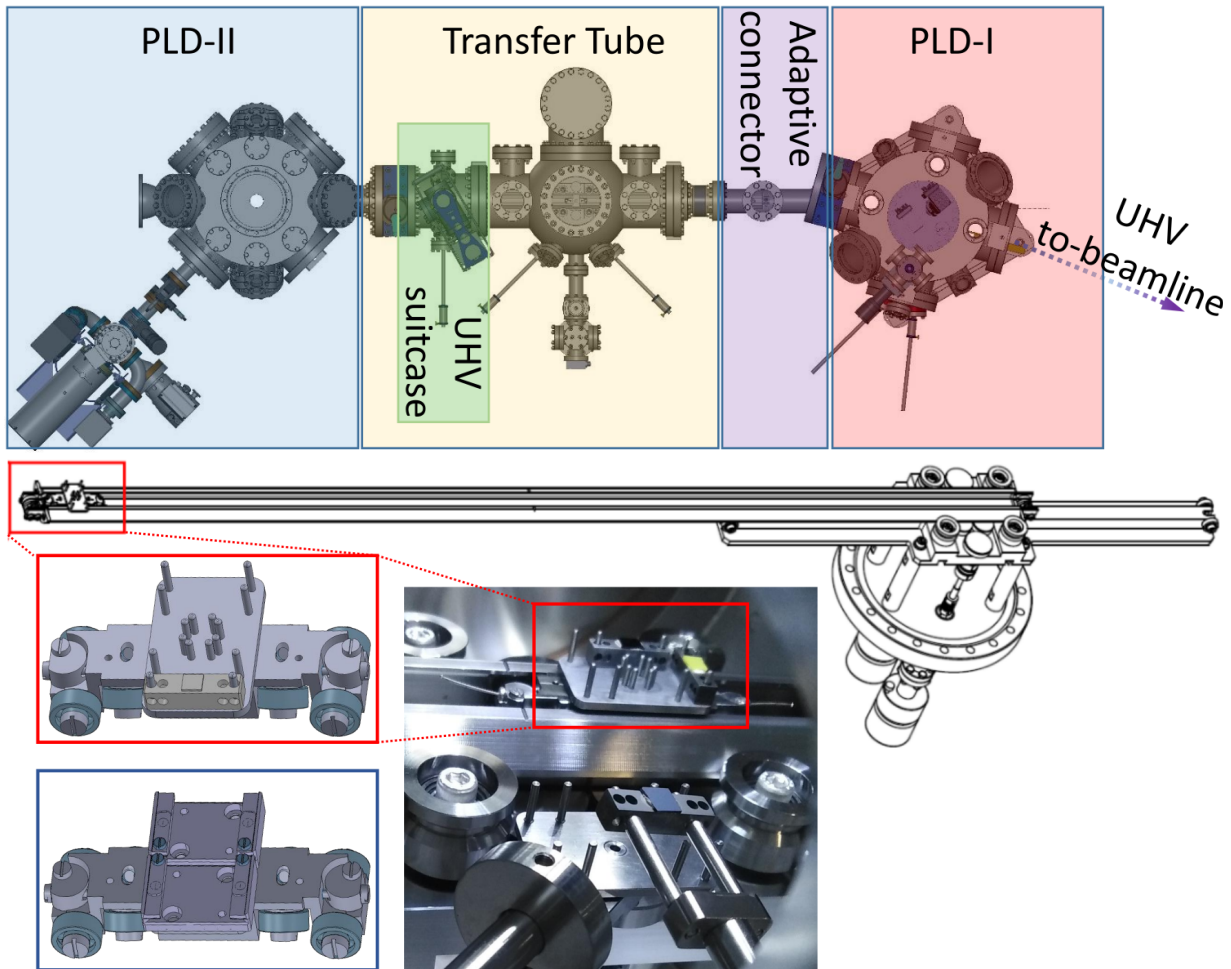
FIG. 1. (upper panel) Top-view representation of the Dual-PLD system: the PLD-I (red), the Transfer Tube (yellow), and the PLD-II (blue) chambers; in particular, within the Transfer Tube, the UHV-suitcase docking position is indicated by a green box; (lower panel) Sketch of the sample transfer mechanism of the Transfer Tube; a zooming-in of the vessel for the APE (red box) and flag-type (blue box) sample holders; a picture of the vessel with the APE sample holders is also reported with several 5 x 5 mm single-crystals glued on top of them.

samples (e.g. angular-resolved photo-emission spectroscopy, scanning tunnel microscopy, low-energy electron diffraction, x-ray absorption and magnetic dichroism, magneto-optical Kerr effect)[18–21]. Such flexibility has been fully used to support a user-driven program for the synthesis of materials in form of thin films and heterostructures[25,26]. The Dual-PLD encompasses the fabrication of a range of several quantum materials with emphasis on the effect of interface properties which are accessible by use of the *digital* approach in thin films and heterostructures. The Dual-PLD provides new viable routes to determine the true nature of the quantum phenomena at the interface/surface of such a class of artificial materials and to precisely craft their physical properties.

II. SYSTEM OVERVIEW

The suite of the UHV-apparatus forming the Dual-PLD system is shown in Figure.1. The two deposition chambers - namely PLD-I and PLD-II - are interconnected by a

home-built UHV bidirectional linear transfer system located in the Transfer Tube[27]. This last is also equipped with a fast-intro UHV chamber for the loading/unloading of the samples and a docking port for the UHV transferring of the samples (e.g. Ferrovac VSN40S). Between the PLD-I and the Transfer Tube, an ad-hoc adaptive connector is present to adjust the main axis of PLD-I with the transfer arm coming from the APE-beamline. A bi-directional transfer rail has been designed and home-built at CNR-IOM and is allocated in the Transfer Tube. The traveling of the vessel is controlled by two independent cranks connected to the bottom flange of the Transfer-Tube (see lower panel of Figure.1); in particular, one allows the moving of a displaceable rail (i.e. in Figure.1 the rail is at its maximum elongation on the right) for a total transfer distance of about 2 m with a UHV envelope limited to only 1.1 m external encumbrance; a second crank allows to move the vessel hosting the sample holders along the entire length of the displaceable rail.

The single crystals for the thin film deposition can be mounted on a variety of sample holders that are heated up by
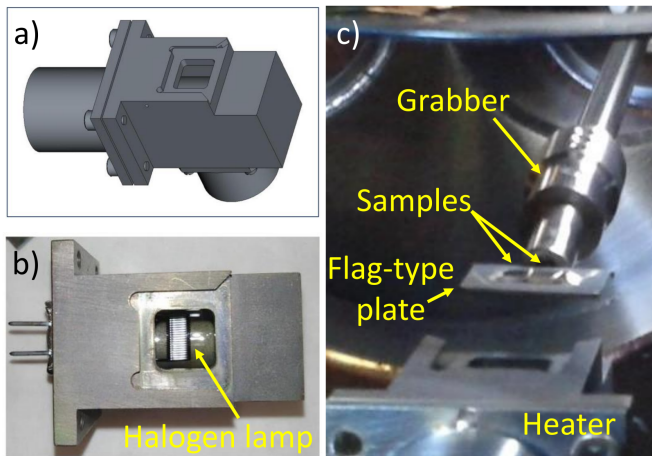
FIG. 2. (a) Sketch of the heating block for flag-type sample holders; (b) top-view picture of the heating block with the position of the DC 400W halogen-lamp with respect to the flag-type sample holder docking slot; (c) picture of loading/unloading of the flag-type plate with two samples glued on top of it.

FIG. 3. Sketch of the deposition chamber (Demcon TSST's target carousel is also included in the sketch[30]); the two independent lasers are focused on the selected target and their paths are enlightened by different colors; in the inset, a zooming in of the target-substrate area with a sketch of the plume.

a DC 400W halogen-lamp generated radiation (e.g. OSRAM 64663HLX - see Figure.2); in particular, for the transferring to the APE end-stations, samples up to 10 x 5 mm lateral dimensions and 0.1-1 mm thickness can be hosted on home-built sample holders; in addition, larger samples (i.e. up to 14 x 14 mm lateral dimensions) can be hosted on flag-type sample holders (e.g. Ferrovac SHOS)[28].

The Dual-PLD system is equipped with two replicas of the same deposition chamber (Figure.3)[29] and it is dedicated to the growth of nanostructured complex materials in form of thin films, multi-layers, and heterostructures. Both the chambers are equipped with a multi-target carousel (namely, pc-remotely controlled 4- and 6-target carousels manufactured by Demcon TSST[30]) for allowing the growth of different materials within the same deposition run. The ablation process is obtained by using an Innolas Spitlight Compact 400–10 Nd:YAG pulsed laser source by means of its first harmonics at 1064 nm and a Coherent COMPex 102-F KrF laser source operating at 248 nm. In particular, the excimer laser source can be used in both the PLD chambers by means of mirrors to guide the laser beam into the depositions chambers. However, only one PLD chamber (namely, the PLD-I) is also equipped with the Nd:YAG laser, with its laser beam being directly guided into the chamber without the use of any mirrors. The pristine spot size of the Nd:YAG laser shot is about 6 mm in diameter with a typical energy of 700 mJ, corresponding to an energy density of about 2.5 J cm^{-2} for the unfocused beam. With the dual aim of avoiding the peripheral region of the laser spots as well as reducing the growth rate per laser shot, an optical mask was used to reduce the spot size from 5 to 2 mm in diameter. Differently, the pristine spot size of the KrF laser shot is about 3 x 1 cm with a typical energy of 340 mJ, corresponding to an energy density of about 0.1 J cm^{-2} for the unfocused beam. By taking advantage of a set of mirrors, both the radiation from the KrF and the Nd:YAG laser can
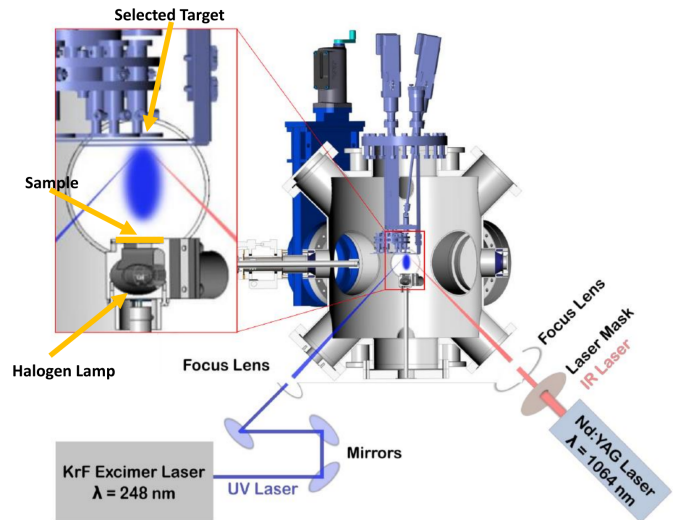
be independently focused on the selected target position. This allows the use of both lasers depending on the specific needs. While both lasers efficiently ablate powders-pressed pellets and single crystals, Nd:YAG laser appears to be more efficient in ablating metal-disk targets (e.g. Fe, Co)[10,31,32]. As a matter of fact, laser sources with short wavelengths are widely utilized to ablate wide band-gap insulators while failing for the ablation of metals due to their small absorption in UV range. However, the possibility to have access to IR solid-state laser in the same chamber extends the range of materials that can be in-situ laser-ablated. One PLD-chamber (namely, PLD-II in Figure.1) is also equipped with a Near-Ambient-Pressure Reflection High Energy Electron Diffraction (NAP-RHEED) system (SPECS NAP-RHEED RHD-30) allowing the in-situ monitoring of the growth up to 1.3 mbar. The base pressure of both the chambers is in the range of 10^{-9} mbar.

III. PERFORMANCES AND RESULTS

In order to assess the flexibility of the Dual-PLD system, we give here two examples of the high-quality, stoichiometric films achievable by alternating the use of the KrF UV and the Nd:YAG IR lasers sources. In particular, FeSe/TiO$_2$ bi-layered heterostructures have been grown on (0 0 1) oriented SrLaAlO$_4$ (SLAO) substrates by using the Nd:YAG laser for the FeSe top-layer and the KrF for the TiO$_2$ buffer-layer. PLD growth of epitaxial FeSe and TiO$_2$ thin films was performed using a stoichiometric poly-crystalline FeSe target (purity 99.99%) and on a rutile TiO$_2$ single crystal. The laser repetition rate was varied from 10 Hz down to 0.1 Hz. Epitaxial growth of FeSe and TiO$_2$ thin films was performed under UHV conditions (i.e. base pressure in the range of 10^{-8} mbar) and in 10^{-4} mbar ultra-pure oxygen background
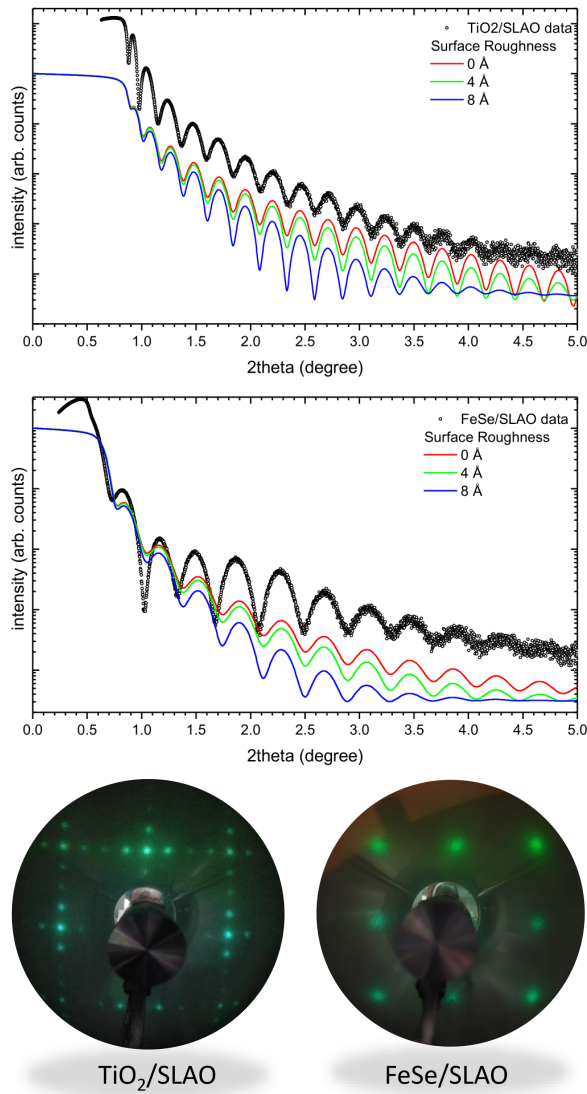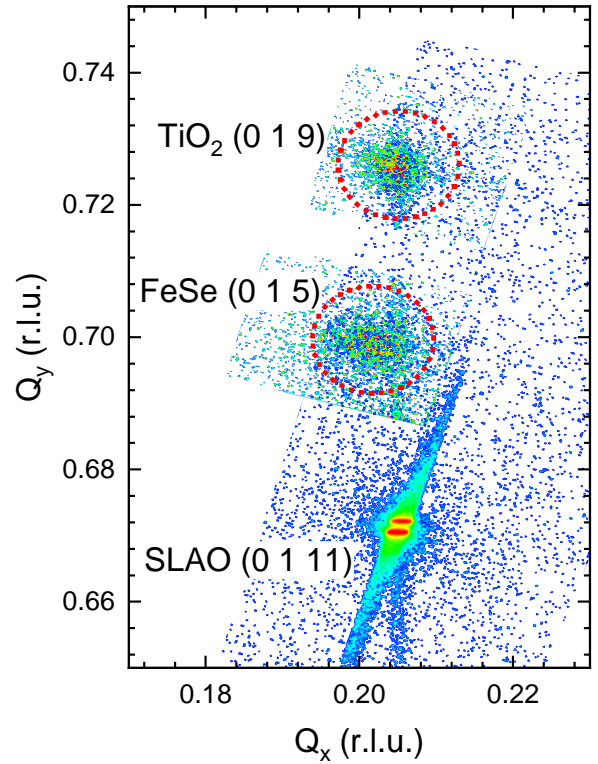
FIG. 5. Reciprocal space maps of a FeSe/TiO$_2$ bilayered heterostructures grown on SLAO substrate around the (0 1 5) FeSe, (0 1 9) TiO$_2$ and (0 1 11) SLAO asymmetric reflections.

FIG. 4. (upper panels) Low-angle x-ray reflectivity scans of a TiO$_2$ and a FeSe thin films grown on SLAO (0 0 1) substrate, respectively; simulations of low-angle x-ray reflectivity is also reported as solid lines; in particular surface roughness values of 0 Å(red), 4 Å(green) and 8 Å(blue) are simulated for all the presented structures; (lower panel) typical LEED pattern of TiO$_2$ and FeSe single-layers grown on SLAO substrate showing the 4 × 1 and 1 × 1 surface reconstructions, respectively.

atmosphere (purity at 99.9999%), respectively. As previously reported[23], the substrate-to-target distance d was set to 10 cm to minimize the presence of FeSe particulates on the film's surface[23,31,32]. After the film growth, both FeSe and TiO$_2$ single layers as well as FeSe/TiO$_2$ bilayered heterostructures were cooled down to room temperature at the base pressure of the chambers in the range of 10^{-8} mbar. Structural characterization of all the films was carried out ex-situ using a four-circle Panalytical X'pert diffractometer with a Cu K$_\alpha$ radiation source. The surface morphology as well as the surface long-range order were investigated in-situ, under UHV

conditions, by atomic-resolution scanning tunnel microscopy (STM) and low-energy electron diffraction (LEED), respectively.

TiO$_2$ thin films were grown by using the KrF excimer pulsed laser source at a typical energy density of about 2 J/cm^{-2} resulting in a deposition rate of about 0.08 Å per laser shot[18,33,34]. The bulk crystallographic properties of the grown samples were explored by means of XRD. In particular, typical $\theta/2\theta$ spectra only show the (0 0 l) peaks, indicating the preferential c-axis orientation of the film along the [0 0 1] substrate crystallographic direction with no trace of impurity phases (not shown here). The surface roughness of the grown films was probed by low-angle x-ray reflectivity (XRR) and reported in the upper panel of Figure.4. Numerical simulations of the low-angle XRR data (i.e., line-curves in Figure.4) were performed by means of the IMD package in the XOP software[35,36]. XRR oscillations are recorded up to 2θ values of 5°, while, above this angle, the oscillations fall below the experimental sensitivity of the x-ray diffractometer[37].

FeSe thin films were grown by using the Nd:YAG pulsed laser source with a typical deposition rate of about 0.13 Å per laser shot[22]. As for the anatase TiO$_2$, also in the case of FeSe, $\theta/2\theta$ spectra only show the (0 0 l) peaks, indicating the preferential c-axis orientation of the film along the [0 0 1] substrate crystallographic direction with no trace of impurity phases (not shown here). Similarly to the previous case, low-angle XRR was performed to evaluate the surface roughness
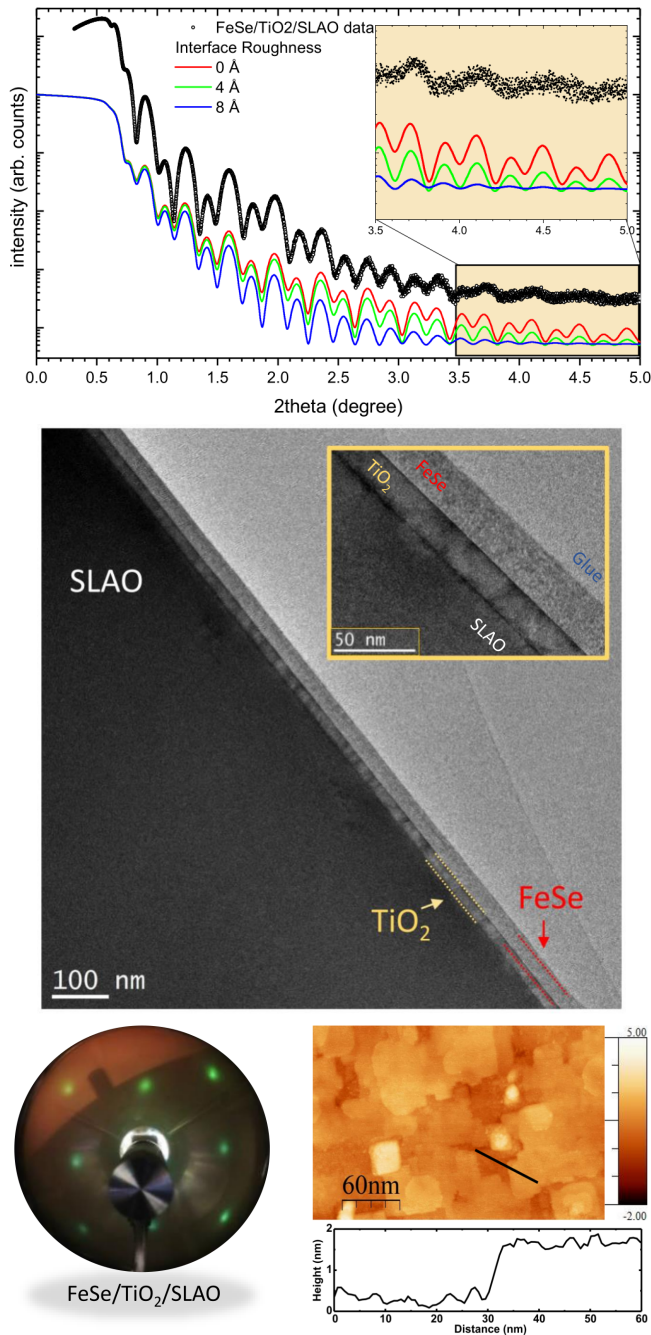
FIG. 6. (upper panel) Low-angle x-ray reflectivity scans of a FeSe/TiO$_2$ bilayered heterostructures grown on SLAO (0 0 1) substrate; simulations of low-angle x-ray reflectivity are also reported as solid lines; in particular surface/interface roughness values of 0 Å(red), 4 Å(green), and 8 Å(blue) are simulated for all the presented structures; (center) BF-TEM image of a FeSe/TiO$_2$ bilayered heterostructure on SLAO substrate (in the inset, zooming out of the interfacial regions); (lower panel) typical LEED pattern of a FeSe/TiO$_2$ bilayered heterostructure showing the 1 × 1 surface reconstruction and STM topography images in the scan area of 300 × 200 nm^2 (the corresponding line-profile is shown below).

of the grown films (middle panel in Figure.4). Also in this

case, XRR oscillations are recorded up to 2θ values of 5° then falling - above it - below the experimental sensitivity of the x-ray diffractometer. The upper limit of the RMS surface roughness was therefore estimated to be about 6 Å.

Even though the XRR fitting algorithm is based on a monochromatized X-ray source with negligible lateral inhomogeneities of the beam (while we used a lab-based unmonochromatized X-ray beam), the surface root-mean-square (RMS) roughness was estimated to be about 6 Å, corresponding to less than one single TiO$_2$ unit cell. Yet such a value must be considered as an upper limit for the surface RMS. As a matter of fact, the actual surface of the thin films was found systematically smaller when probed by in-situ scanning tunnel microscopy[18,20,37,38]. Nevertheless, the results of the XRR analysis provided a structural characterization of the samples on a millimeter scale rather than a micrometer one.

Finally FeSe/TiO$_2$ bilayered heterostructures were grown by using the combination of both laser sources. In particular, the TiO$_2$ buffer-layer was deposited at 700° and 10^{-4} mbar of oxygen pressure, then the grown film was cooled down in UHV-condition to 300° and then the FeSe top-layer deposition was performed.

XRD θ–2θ scans showed both the layers films have a (0 0 l) orientation, pointing a preferential growth direction along the c-axis (not reported here). The in-plane epitaxial relationship between the FeSe top-layer, TiO$_2$ buffer layer, and the SLAO substrate is determined by reciprocal space maps around the (0 1 5), (0 1 9) and (0 1 11) asymmetric reflections, respectively (Figure.5). The diffraction intensities of the TiO$_2$ buffer-layer and the SLAO substrate do align along the same in-plane scattering vector Q$_x$, confirming that the full strain condition for the TiO$_2$ buffer-layer. However, the maximum of the diffraction peak related to the FeSe top-layer is slightly centered at lower Q$_x$ (i.e. corresponding to a slightly larger in-plane lattice parameter), confirming the tendency of FeSe to structurally relax after a few layers[22].

Besides the thickness of the constituent layers, XRR simulation provided an estimate of the interface roughness between them (Figure.6). Again, XRR oscillations are recorded up to 2θ values of 5° thus inferring to a very low interface roughness and a negligible amount of chemical interdiffusion among the layers.

Nanostructures of FeSe/TiO$_2$ bilayered heterostructures were investigated by Bright-Field Transmission Electron Microscopy (BF-TEM) using a JEOL 2010 UHR TEM equipped with a field emission gun and operated at 200 kV. Cross-sectional TEM samples were prepared with a conventional polishing technique followed by dimpling and milling with Ar ions. This preparation procedure had been proven to minimize structural and chemical modifications of cross-sectional TEM samples and had successfully been applied to other oxide thin-film systems[34,39,40]. The structure of the heterostructure over the whole image is homogeneous, with a very smooth surface and free of significant defects (Figure.6). No structural differences were detected among the near-interface region and far from it, as well as no traces of spurious phases or segregation of crystalline phases other than those expected.

Similarly to FeSe and TiO$_2$ single layers, the surface long-

TABLE I. Materials grown by Dual-PLD during 2017-2022 period according to the research framework within which the synthesis has been performed, namely In-house activity, and the NFFA-Trieste and NFFA-Europe user programs (RE and TM stand for Rare-Earth and Transition-Metal, respectively; asterisks indicate the materials for which the growth protocol has been developed on-demand).

In-house activity	NFFA-Trieste		NFFA-Europe
Bi_2Se_3[12,37,41]	*Dy-doped $SrTiO_3$	*FeTe	*V_2O_3[42–44]
TiO_2[18,45]	*$SrNbO_3$[33,38]	*$Fe(Te_{0.5}Se_{0.5})$	*Fe-doped TiO_2
$SrRuO_3$[46]	*$YBa_2Cu_3O_7$	*Fe	*TM-doped $SrTiO_3$
$La_{0.7}Ba_{0.3}MnO_3$[47]	*$LaNiO_3$[48]	*$MnSe_2$	*$BaTiO_3$
$La_{0.7}Ce_{0.3}MnO_3$[47]	*WO_3	*MoS_2	*RE-doped CeO_2[49,50]
$La_{0.7}Sr_{0.3}MnO_3$	*$LaVO_3$	*Fe_3O_4	*RE-doped MgO
$BiFeO_3$	*ZnO	*$MgGa_2O_4$	*FeSe[22]
Cr_4Te_5	*CeO_2	*$MgCr_2O_4$	*YSZ-8%
	*$LaAlO_3$	*Bi_2WO_6	
	*$CaMnO_3$		

range order was probed in-situ by LEED on a freshly grown $FeSe/TiO_2$ bilayered heterostructure, shown in Figure.6. The LEED pattern acquired at about 100 eV incident electron energy displays sharp diffraction spots with a four-fold symmetry square lattice along the substrate surface cell edge. Interestingly, the TiO_2 (4 x 1) surface reconstruction appears not to induce any surface reconstruction in the FeSe top-layer. Finally, the surface topography and surface roughness of the $FeSe/TiO_2$ bilayered heterostructure were determined by in-situ room temperature STM measurements. STM topography image of the scan area (200 x 300) nm^2 (Figure.6) reveals atomically flat terraces and uniformly distributed with a step height of ~ 1.2 nm, i.e., equivalent to the height of about one TiO_2 or two FeSe unit cells. Such a value is consistent with the RMS obtained from the XRR analysis performed on a millimeter scale. The occurrence of atomically flat surfaces and the absence of spurious extra phases make these films ideal candidates to investigate the intrinsic physical properties of $FeSe/TiO_2$ heterostructures as a function of constituent layers.

IV. CONCLUSIONS

The Dual-PLD system here described allows exploiting the large structural flexibility of thin films to highlight the role of the electronic correlations in quantum materials as a function of several controlled parameters (e.g. dimensionality, chemistry, strain, thickness). The combining use of two independent laser sources - namely a KrF UV and a Nd:YAG IR lasers - has allowed us to successfully grow a large number of different materials - ranging from oxides to metals, to selenides and others - in the form of thin films and heterostructures. During a 2017-2022 five-year period, the Dual-PLD facility has been used to grow 36 different materials in form of thin films and/or heterostructures (Table 1). Such flexibility has been fully used to support a user-driven program for the synthesis of materials in form of thin films and heterostructures. As a matter of

fact, the largest part of its scientific activity has been triggered by external users and has mostly involved the development of previously unknown growth protocols (indicated by asterisks in Table 1). The Dual-PLD system provides new viable routes to unique samples and combinations for the research of the nature to unambiguously determine the true nature of the quantum phenomena at the interface/surface of a vast class of artificial materials and, consequently, to precisely craft their physical properties.

DATA AVAILABILITY STATEMENT

The scientific data that support the findings of this study are available from the corresponding author upon reasonable request.

Technical drawings and specifications of all of the non-commercial pieces of equipment - namely the deposition chamber, the transfer tube, the UHV transfer arm, and the flag-type heating block- are available on the NFFA-Trieste repository of free-to-use design data of advanced instrumentation for nanoscience[51].

The figure of the target carousel manufactured by Demcon TSST in Figure 3 was used under their permission.

CONFLICTS OF INTEREST

The authors have no conflicts to disclose.

REFERENCES

[1] Y. Tokura, M. Kawasaki, and N. Nagaosa, "Emergent functions of quantum materials," Nature Physics 13, 1056–1068 (2017).

[2] H. Y. Hwang, Y. Iwasa, M. Kawasaki, B. Keimer, N. Nagaosa, and Y. Tokura, "Emergent phenomena at oxide interfaces," Nature Materials 11, 103–113 (2012).

[3] A. Tarancón and N. Pryds, "Functional Oxide Thin Films for Advanced Energy and Information Technology," Advanced Materials Interfaces 6, 1900990 (2019).

[4] M. Coll, J. Fontcuberta, M. Althammer, M. Bibes, H. Boschker, A. Calleja, G. Cheng, M. Cuoco, R. Dittmann, B. Dkhil, I. El Baggari, M. Fanciulli, I. Fina, E. Fortunato, C. Frontera, S. Fujita, V. Garcia, S. T. Goennenwein, C. G. Granqvist, J. Grollier, R. Gross, A. Hagfeldt, G. Herranz, K. Hono, E. Houwman, M. Huijben, A. Kalaboukhov, D. J. Keeble, G. Koster, L. F. Kourkoutis, J. Levy, M. Lira-Cantu, J. L. MacManus-Driscoll, J. Mannhart, R. Martins, S. Menzel, T. Mikolajick, M. Napari, M. D. Nguyen, G. Niklasson, C. Paillard, S. Panigrahi, G. Rijnders, F. Sánchez, P. Sanchis, S. Sanna, D. G. Schlom, U. Schroeder, K. M. Shen, A. Siemon, M. Spreitzer, H. Sukegawa, R. Tamayo, J. van den Brink, N. Pryds, and F. M. Granozio, "Towards Oxide Electronics: a Roadmap," Applied Surface Science 482, 1–93 (2019).

[5] D. G. Schlom, L.-Q. Chen, X. Pan, A. Schmehl, and M. A. Zurbuchen, "A Thin Film Approach to Engineering Functionality into Oxides," Journal of the American Ceramic Society 91, 2429–2454 (2008).

[6] S. O. Mbam, S. E. Nwonu, O. A. Orelaja, U. S. Nwigwe, and X.-F. Gou, "Thin-film coating; historical evolution, conventional deposition technologies, stress-state micro/nano-level measurement/models and prospects projection: a critical review," Materials Research Express 6, 122001 (2019).

[7] D. P. Norton, "Synthesis and properties of epitaxial electronic oxide thin-film materials," Materials Science and Engineering: R: Reports 43, 139–247 (2004).

[8] R. K. Singh and J. Narayan, "Pulsed-laser evaporation technique for deposition of thin films: Physics and theoretical model," Physical Review B 41, 8843–8859 (1990).

[9] P. R. Willmott and J. R. Huber, "Pulsed laser vaporization and deposition," Reviews of Modern Physics 72, 315–328 (2000).

[10] C. W. Schneider and T. Lippert, "Laser Ablation and Thin Film Deposition," in Laser Processing of Materials (Springer Berlin, Heidelberg, Germany, 2010) pp. 89–112.

[11] C. Aruta and A. Tebano, "Thin Films and Superlattice Synthesis," in Perovskites and Related Mixed Oxides (Wiley-VCH Verlag GmbH & Co. KGaA, Weinheim, Germany, 2015) pp. 143–168.

[12] P. Orgiani, C. Aruta, G. Balestrino, D. Born, L. Maritato, P. G. Medaglia, D. Stornaiuolo, F. Tafuri, and A. Tebano, "Direct measurement of sheet resistance $R_\square$ in cuprate systems: Evidence of a fermionic scenario in a metal-insulator transition," Physical Review Letters 98, 036401 (2007).

[13] G. Koster, L. Klein, W. Siemons, G. Rijnders, J. S. Dodge, C.-B. Eom, D. H. A. Blank, and M. R. Beasley, "Structure, physical properties, and applications of SrRuO3 thin films," Reviews of Modern Physics 84, 253–298 (2012).

[14] P. Kelly and R. Arnell, "Magnetron sputtering: a review of recent developments and applications," Vacuum 56, 159–172 (2000).

[15] C. Schlueter, P. Orgiani, T.-L. Lee, A. Y. Petrov, A. Galdi, B. A. Davidson, J. Zegenhagen, and C. Aruta, "Evidence of electronic band redistribution in $La_{0.65}Sr_{0.35}MnO_{3-\delta}$ by hard x-ray photoelectron spectroscopy," Physical Review B 86, 155102 (2012).

[16] J. M. Rondinelli and S. J. May, "Instrumental insights," Nature Materials 11, 833–834 (2012).

[17] C. W. Schneider and T. Lippert, "ChemInform Abstract: Laser Ablation and Thin Film Deposition," ChemInform 42, no–no (2011).

[18] B. Gobaut, P. Orgiani, A. Sambri, E. di Gennaro, C. Aruta, F. Borgatti, V. Lollobrigida, D. Céolin, J.-P. Rueff, R. Ciancio, C. Bigi, P. K. Das, J. Fujii, D. Krizmancic, P. Torelli, I. Vobornik, G. Rossi, F. Miletto Granozio, U. Scotti di Uccio, and G. Panaccione, "Role of Oxygen Deposition Pressure in the Formation of Ti Defect States in TiO_2 (001) Anatase Thin Films," ACS Applied Materials and Interfaces 9, 23099–23106 (2017).

[19] C. Bigi, P. Orgiani, J. Słavińska, J. Fujii, J. T. Irvine, S. Picozzi, G. Panaccione, I. Vobornik, G. Rossi, D. Payne, and F. Borgatti, "Direct insight into the band structure of SrNbO3," Physical Review Materials 4, 025006 (2020).

[20] F. Mazzola, S. K. Chaluvadi, V. Polewczyk, D. Mondal, J. Fujii, P. Rajak, M. Islam, R. Ciancio, L. Barba, M. Fabrizio, G. Rossi, P. Orgiani, and I. Vobornik, "Disentangling Structural and Electronic Properties in V_2O_3 Thin Films: A Genuine Nonsymmetry Breaking Mott Transition," Nano Letters 37, C4–199–C4–205 (2022).

[21] P. Orgiani, C. Bigi, P. Kumar Das, J. Fujii, R. Ciancio, B. Gobaut, A. Galdi, C. Sacco, L. Maritato, P. Torelli, G. Panaccione, I. Vobornik, and G. Rossi, "Structural and electronic properties of Bi_2Se_3 topological insulator thin films grown by pulsed laser deposition," Applied Physics Letters 110, 171601 (2017).

[22] S. K. Chaluvadi, D. Mondal, C. Bigi, J. Fujii, R. Adhikari, R. Ciancio, A. Bonanni, G. Panaccione, G. Rossi, I. Vobornik, and P. Orgiani, "Direct-ARPES and STM Investigation of FeSe Thin Film Growth by Nd:YAG Laser," Coatings 11, 276 (2021).

[23] S. K. Chaluvadi, D. Mondal, C. Bigi, D. Knez, P. Rajak, R. Ciancio, J. Fujii, G. Panaccione, I. Vobornik, G. Rossi, and P. Orgiani, "Pulsed laser deposition of oxide and metallic thin films by means of Nd:YAG laser source operating at its 1st harmonics: recent approaches and advances," Journal of Physics: Materials 4, 032001 (2021).

[24] G. Panaccione, I. Vobornik, J. Fujii, D. Krizmancic, E. Annese, L. Giovanelli, F. Maccherozzi, F. Salvador, A. De Luisa, D. Benedetti, A. Gruden, P. Bertoch, F. Polack, D. Cocco, G. Sostero, B. Diviacco, M. Hochstrasser, U. Maier, D. Pescia, C. H. Back, T. Greber, J. Osterwalder, M. Galaktionov, M. Sancrotti, and G. Rossi, "Advanced photoelectric effect experiment beamline at Elettra: A surface science laboratory coupled with Synchrotron Radiation," Review of Scientific Instruments 80, 043105 (2009).

[25] NFFA-Trieste access is performed via the website, https://www.trieste.nffa.eu .

[26] NFFA.eu Pilot access is performed via the website, https://www.nffa.eu .

[27] Transfer-Tube open-access instrumentation of NFFA-Trieste, https://www.trieste.nffa.eu/nanoshow/uhv-linear-transfer-system/ .

[28] Flag-style radiative heater open-access instrumentation of NFFA-Trieste, https://www.trieste.nffa.eu/nanoshow/heater-for-flag-style-sample-holders/ .

[29] Dual-PLD chambers open-access instrumentation of NFFA-Trieste, https://www.trieste.nffa.eu/nanoshow/dual-pld-system/ .

[30] Demcon TSST, Developer and manufacturer of thin film equipment, https://tsst.demcon.com .

[31] A. Tselev, A. Gorbunov, and W. Pompe, "Spatio-energetical characteristics of laser plasma in cross-beam pulsed laser deposition," Applied Surface Science 138-139, 12–16 (1999).

[32] A. Tselev, A. Gorbunov, and W. Pompe, "Cross-beam pulsed laser deposition: General characteristic," Review of Scientific Instruments 72, 2665–2672 (2001).

[33] C. Bigi, Z. Tang, G. M. Pierantozzi, P. Orgiani, P. K. Das, J. Fujii, I. Vobornik, T. Pincelli, A. Troglia, T.-L. Lee, R. Ciancio, G. Drazic, A. Verdini, A. Regoutz, P. D. C. King, D. Biswas, G. Rossi, G. Panaccione, and A. Selloni, "Distinct behavior of localized and delocalized carriers in anatase TiO_2 (001) during reaction with O_2," Physical Review Materials 4, 025801 (2020).

[34] D. Knez, G. Dražić, S. K. Chaluvadi, P. Orgiani, S. Fabris, G. Panaccione, G. Rossi, and R. Ciancio, "Unveiling Oxygen Vacancy Superstructures in Reduced Anatase Thin Films," Nano Letters 20, 6444–6451 (2020).

[35] M. Sánchez del Río and R. J. Dejus, "XOP v2.4: recent developments of the x-ray optics software toolkit," (2011) p. 814115.

[36] D. L. Windt, "IMD—Software for modeling the optical properties of multilayer films," Computers in Physics 12, 360 (1998).

[37] C. Bigi, P. Orgiani, A. Nardi, A. Troglia, J. Fujii, G. Panaccione, I. Vobornik, and G. Rossi, "Robustness of topological states in Bi_2Se_3 thin film grown by Pulsed Laser Deposition on (001)-oriented SrTiO3 perovskite," Applied Surface Science 473, 190–193 (2019).

[38] P. Di Pietro, C. Bigi, S. K. Chaluvadi, D. Knez, P. Rajak, R. Ciancio, J. Fujii, F. Mercuri, S. Lupi, G. Rossi, F. Borgatti, A. Perucchi, and P. Orgiani, "Oxygen-Driven Metal–Insulator Transition in $SrNbO_3$ Thin Films Probed by Infrared Spectroscopy," Advanced Electronic Materials 8, 2101338 (2022).

[39] R. Ciancio, E. Carlino, C. Aruta, D. Maccariello, F. M. Granozio, and U. Scotti di Uccio, "Nanostructure of buried interface layers in TiO_2 anatase thin films grown on $LaAlO_3$ and $SrTiO_3$ substrates," Nanoscale 4, 91–94 (2012).

[40] P. Rajak, D. Knez, S. K. Chaluvadi, P. Orgiani, G. Rossi, L. Méchin, and R. Ciancio, "Evidence of Mn-ion structural displacements correlated with oxygen vacancies in $La_{0.7}Sr_{0.3}MnO_3$ interfacial dead layers," ACS Applied Materials and Interfaces 13, 55666–55675 (2021).

[41] R. Gracia-Abad, S. Sangiao, C. Bigi, S. Kumar Chaluvadi, P. Orgiani, and J. M. De Teresa, "Omnipresence of Weak Antilocalization (WAL) in Bi2Se3 Thin Films: A Review on Its Origin," Nanomaterials 11, 1077 (2021).

[42] M. Caputo, J. Jandke, E. Cappelli, S. K. Chaluvadi, E. Bonini Guedes, M. Naamneh, G. Vinai, J. Fujii, P. Torelli, I. Vobornik, A. Goldoni, P. Orgiani, F. Baumberger, M. Radovic, and G. Panaccione, "Metal to insulator transition at the surface of V_2O_3 thin films: An in-situ view," Applied Surface Science 574, 151608 (2022).

[43] V. Polewczyk, S. K. Chaluvadi, P. Orgiani, G. Panaccione, G. Vinai, G. Rossi, and P. Torelli, "Tuning the magnetic properties of V_2O_3/CoFeB heterostructures across the V_2O_3 structural transition," Physical Review Materials 5, 034413 (2021).

[44] V. Polewczyk, S. Chaluvadi, D. Dagur, F. Mazzola, S. Punathum Chalil, A. Petrov, J. Fujii, G. Panaccione, G. Rossi, P. Orgiani, G. Vinai, and P. Torelli, "Chemical, structural and electronic properties of ultrathin V2O3 films on Al2O3 substrate: Implications in Mott-like transitions," Applied Surface Science 610, 155462 (2023).

[45] A. Troglia, C. Bigi, I. Vobornik, J. Fujii, D. Knez, R. Ciancio, G. Dražić, M. Fuchs, D. D. Sante, G. Sangiovanni, G. Rossi, P. Orgiani, and G. Panaccione, "Evidence of a 2D Electron Gas in a Single-Unit-Cell of Anatase TiO_2 (001)," Advanced Science 9, 2105114 (2022).

[46] A. Nardi, C. Bigi, S. K. Chaluvadi, R. Ciancio, J. Fujii, I. Vobornik, G. Panaccione, G. Rossi, and P. Orgiani, "Analysis of Metal-Insulator Crossover in Strained $SrRuO_3$ Thin Films by X-ray Photoelectron Spectroscopy," Coatings 10, 780 (2020).

[47] C. Bigi, S. K. Chaluvadi, A. Galdi, L. Maritato, C. Aruta, R. Ciancio, J. Fujii, B. Gobaut, P. Torelli, I. Vobornik, G. Panaccione, G.Rossi, and P. Orgiani, "Predominance of z^2-orbitals at the surface of both hole- and electron-doped manganites," Journal of Electron Spectroscopy and Related Phenomena 245, 147016 (2020).

[48] P. Di Pietro, M. Golalikhani, K. Wijesekara, S. K. Chaluvadi, P. Orgiani, X. Xi, S. Lupi, and A. Perucchi, "Spectroscopic evidence of a dimensionality-induced Metal-to-Insulator Transition in the Ruddlesden–Popper $La_{n+1}Ni_nO_{3n+1}$ series," ACS Applied Materials and Interfaces 13, 6813–6819 (2021).

[49] N. Yang, P. Orgiani, E. Di Bartolomeo, V. Foglietti, P. Torelli, A. V. Ievlev, G. Rossi, S. Licoccia, G. Balestrino, S. V. Kalinin, and C. Aruta, "Effects of Dopant Ionic Radius on Cerium Reduction in Epitaxial Cerium Oxide Thin Films," Journal of Physical Chemistry C 121, 8841–8849 (2017).

[50] N. Yang, D. Knez, G. Vinai, P. Torelli, R. Ciancio, P. Orgiani, and C. Aruta, "Improved Structural Properties in Homogeneously Doped $Sm_{0.4}Ce_{0.6}O_{2-\delta}$ Epitaxial Thin Films: High Doping Effect on the Electronic Bands," ACS Applied Materials and Interfaces 12, 47556–47563 (2020).

[51] NFFA Nano-show open-access instrumentation, https://www.trieste.nffa.eu/nanoshow/ .